Thermal Bistability of an Ultrathin Film of Iron(II) Spin-Crossover Molecules Directly Adsorbed on a Metal Surface

Massine Kelai, Vincent Repain, Arthur Tauzin, Weibin Li, Yann Girard, Jérôme Lagoute, Sylvie Rousset, Edwige Otero, Philippe Sainctavit, Marie-Anne Arrio, et al.

Thermal Bistability of an Ultrathin Film of Iron(II) Spin-Crossover Molecules Directly Adsorbed on a Metal Surface

Massine Kelai,[†] Vincent Repain,[†] Arthur Tauzin,[‡] Weibin Li,[¶] Yann Girard,[†] Jérôme Lagoute,[†] Sylvie Rousset,[†] Edwige Otero,[§] Philippe Sainctavit,[§,¶] Marie-Anne Arrio,[¶] Marie-Laure Boillot,[‡] Talal Mallah,[‡] Cristian Enachescu,[‖] and Amandine Bellec*[,†]

†*Matériaux et Phénomènes Quantiques, Université de Paris, CNRS UMR 7162, 75013 Paris, France*

‡*Institut de Chimie Moléculaire et des Matériaux d'Orsay, Univ Paris Sud, Université Paris-Saclay, CNRS, UMR 8182, 91405 Orsay Cedex, France*

¶*Institut de Minéralogie, de Physique des Matériaux et de Cosmochimie, CNRS UMR7590, Sorbonne Université, MNHN, 75252 Paris Cedex 5, France*

§*Synchrotron SOLEIL, L'Orme des Merisiers, Saint-Aubin, 91192 Gif sur Yvette, France*

‖*Faculty of Physics, Alexandru Ioan Cuza University of Iasi, Iasi 700506, Romania*

E-mail: amandine.bellec@u-paris.fr

Abstract

Spin-crossover molecules are very attractive compounds to realize multifunctional spintronic devices. Understanding their properties when deposited on metals is therefore crucial for their future rational implementation as ultrathin films in such devices. Using X-ray absorption spectroscopy, we study the thermal transition of the spin-crossover compound $Fe^{II}((3,5\text{-}(CH_3)_2Pz)_3BH)_2$ from submonolayer to multilayers on a Cu(111) substrate. We determine how the residual fraction of high spin molecules at low temperature as well as the bistability range and the temperature of switching depend on the layer thickness. The most spectacular effect is the clear opening of a 35±9 K thermal hysteresis loop for a 3.0±0.7 monolayers thick film. In order to better understand the role played by the substrate and the dimensionality on the thermal bistability, we have performed Monte Carlo Arrhenius simulations in the framework of a mechanoelastic model that include a molecule-substrate interaction. This model reproduces well the main features observed experimentally and can predict how the spin-crossover transition is modified by the thickness and the substrate interaction.

Graphical TOC Entry

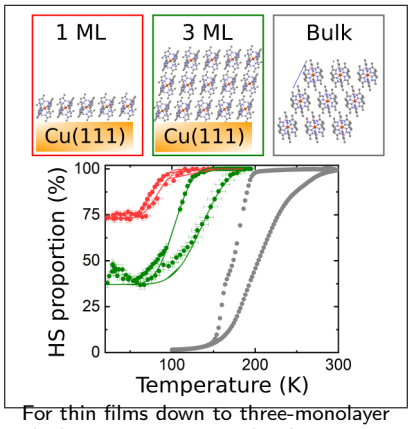

For thin films down to three-monolayer thick, spin-crossover molecules present an thermal hysteresis when adsorbed on Cu(111).

Keywords

Spin-Crossover, Thermal Bistability, X-ray Absorption Spectroscopy, Mechanoelastic Model

Spin-crossover (SCO) molecules are promising systems for the development of molecular spintronics,[1] as they present two electronic spin states that can be controlled by external stimuli such as light, pressure or temperature.[2–4] Fe^{II} based SCO molecules are the most synthesized and studied in the literature.[4,5] Their electronic structure ($3d^6$ configuration) is characterized by their low-spin state (LS, t_{2g}^6 e_g^0, S = 0) and high-spin state (HS, t_{2g}^4 e_g^2, S = 2). The thermal induced switching process between HS and LS is well documented for bulk materials.[6] This property mediated by phonon and electron-phonon coupling can be accompanied by the observation of a thermal hysteresis loop which is a manifestation of bistability or the so called 'memory-effect'. In the hysteresis range, the two spin states can be considered as being associated with binary code (ON/OFF) and this can be used for example for the conception of molecular memory devices.[7–9] However, it remains relatively uncommon and unpredictable to get an hysteresis of more than a few Kelvin.[6] Inserting them in spintronic devices remains a big challenge for future applications[10,11] and requires a deep understanding of their properties in the form of nanoparticules,[8,12–14] ultrathin films[15–18] and down to a single layer on various substrates.[19,20] In addition, the structural distortions that accompany the volume change in the spin-state switching produce elastic strains manifested by short and long-range interactions and cooperative transformations. The cooperativity is a key parameter to understand the thermal spin-transition behavior (transition temperature, shape and width of the thermal bistability, residual high spin fraction at low temperature). It was unveiled that the shape of the thermal transition is size-dependant[21] and can significantly differ from the bulk one in thin films or nanoparticles.[22–25] It was also shown that the molecule-substrate interaction is generally responsible for an incomplete transition, with a residual proportion of HS molecules at low temperature that can be ascribed to epitaxial strain and a related loss of cooperativity.[19,20,26–28]

In order to have a qualitative and quantitative description of the effect of cooperativity, many methods have been proposed in the past such as Ising-like or Slichter-Drickamer mean field models.[29,30] Unfortunately, these methods failed to describe some microscopic experimen-

tal features of the thermal transition such as nucleation-propagation of spin like domains. For this purpose, a new class of models has been elaborated, by replacing the ambiguous short-range and long-range interactions by elastic interactions arising from lattice distortions. Monte Carlo Arrhenius simulations based on a 3D mechanoelastic model enable to capture finer details of the SCO system. This theoretical tool has been applied successfully to describe the thermal bistability in macroscopic crystals and also loss of cooperativity for SCO nanoparticles adsorbed on substrates.[31]

In this paper, we study ultrathin films of $Fe^{II}((3,5\text{-}(CH_3)_2Pz)_3BH)_2$, Pz=pyrazolyl, called **(1)** in the following. This molecule is sublimable under ultra-high-vacuum (UHV) conditions and was found to be robust against decomposition when adsorbed on different metals.[20] It also retained its switching ability down to the submonolayer coverage, while with drastic changes as compared to the bulk behavior.[20,26,32] Using X-ray absorption spectroscopy, we demonstrate that **(1)** exhibits a clear thermal bistability for ultrathin films as thin as 3 nm deposited on metallic substrate, what is of high interest for vertical electronic devices. By using mechanoelastic simulations including the substrate, we can reproduce this bistability for such thin films and also explain quantitatively how the HS residual and the transition temperature evolve as function of the thickness.

Soft X-ray absorption spectroscopy (XAS) is a very powerful tool to investigate the electronic and magnetic properties at the level of SCO molecule-substrate interfaces. The Fe^{II} L_3 absorption edge spectral profile is a fingerprint of the spin state of the SCO molecule and provides quantitative information on the spin conversion. Figure 1 shows XA spectra taken at high temperature and low temperature for three different coverages of **(1)** on a Cu(111) surface. Other coverages and temperatures are available in Supporting Information (SI). At high temperature, the spectra measured for all coverages are typical of a full HS with the main characteristic peak at 707.9 eV, as expected for a bulk material at 300 K. As the temperature decreases, the HS peak decreases and the characteristic LS peak at 709.2 eV increases.

At low temperature, two striking observations can be done from those spectra. Firstly, the molecular layer never shows a pure LS phase at low temperature, in contrast to what is observed in bulk,[24,33] but a mixture of HS and LS. Such a spin-state mixing has already been observed for **(1)** on metallic surfaces[20] or for other surface-supported molecules.[19,34,35] For the adsorption of a submonolayer of molecules **(1)** on Au(111), the incomplete transition originates from the epitaxial relationship between the substrate and the molecular layer.[26] Secondly, at low temperature the HS to LS conversion is more efficient for higher thickness. To extract the fraction of HS molecules as a function of temperature $x_{HS}(T)$, we adjust

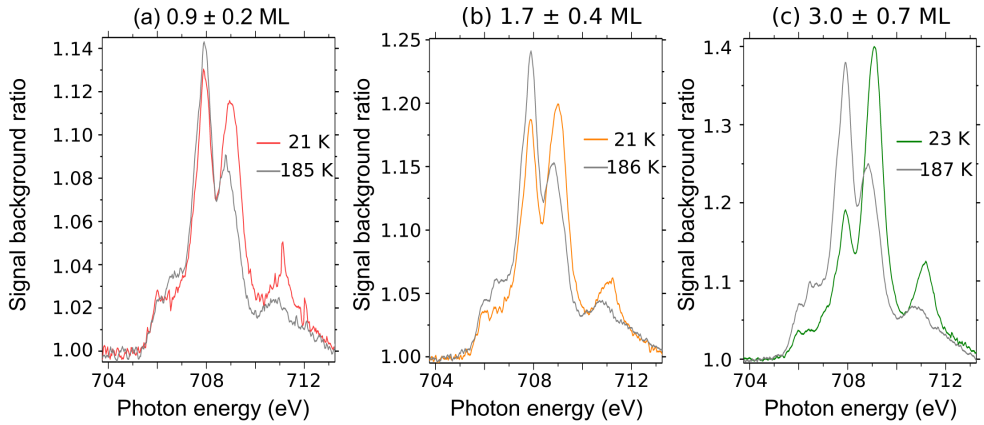

Figure 1: Normalized XAS signal at L_3 edge of Fe^{II} of **(1)** on Cu(111) recorded at low temperature (colored) and high temperature (grey). (a): 0.9±0.2 ML; (b): 1.7±0.4 ML; (c): 3.0±0.7 ML. A linear background has been subtracted for all the spectra and the signal is normalized to the background value at 707.9 eV.

the experimental spectra by a linear combination of pure HS and LS reference spectra (the fitted data are shown as movies in SI). The reference HS and LS spectra are taken from bulk materials (cf. SI for more details). Figure 2 presents the evolution of x_{HS} as a function of the temperature for different thicknesses, and are compared to the bulk behavior, extracted from a magnetic susceptibility measurement.[33] A thermal ramp of 1 $K.min^{-1}$ is imposed by first raising and then lowering the temperature. For all these curves, the left branch (resp. right) of the hysteresis curve corresponds to the descending (resp. ascending) branch in temperature as it is shown for the bulk.

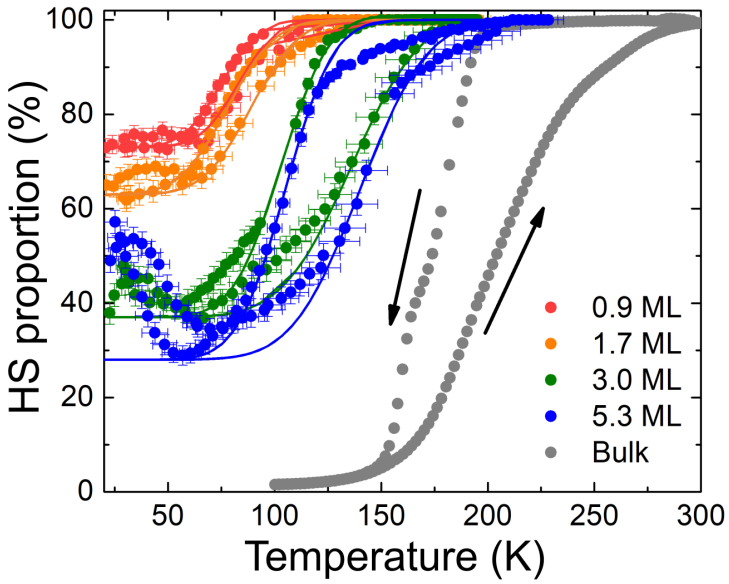

Figure 2: HS proportion as function of temperature. Red: 0.9±0.2 ML; Orange: 1.7±0.4 ML; Green: 3.0±0.7 ML; Blue: 5.3±1.3 ML; Grey: bulk extracted from a susceptibility measurement. The solid lines are guides to the eye using an error function.

In order to ensure that the opening of a thermal hysteresis was not due to a systematic error on the sample temperature, we have first decided to realize three different molecular thicknesses (0.9 ML, 1.7 ML and 3.0 ML, ML denoting the molecular monolayer) on the same Cu(111) single crystal (see methods). Similarly, the 3.8 ML (see SI) and 5.3 ML thicknesses have been recorded concomitantly. Thus, on the same sample, the differences in the switching properties can be directly ascribed to the different thicknesses and not to possible differences in the thermal contact of the samples. Moreover, we have taken great care to correct accurately the measured temperature. Indeed, for technical reasons, the sample is few centimeters away from the temperature probe. The given temperature is therefore a corrected temperature using a calibration procedure based on a thermal diffusion model, detailed in SI. Typically, this correction reduces the hysteresis for the 0.9 ML thickness from 20 K for the uncorrected data to 11±9 K for the corrected data (cf. SI).

We have extracted three important quantities from those curves: the residual fraction of HS molecules at low temperature (x_{HS}^{res}), the transition temperature (T_{tr}) and the width of bistability (ΔT). The last two quantities are defined by looking at the intersection of $\frac{1+x_{HS}^{res}}{2}$

with the hysteresis curves. We obtain two temperatures, namely T_{up} and T_{down}, with T_{tr} the average and ΔT the difference.

One can directly observe in Figure 2 that the thicker the film, the lower x_{HS}^{res} and the higher T_{tr} (see SI for the determined values). For the temperature range below 50 K, the rising of HS proportion is certainly due to SOXIESST effects (Soft X-ray Induced Excited Spin State Trapping)[36] - especially for higher thicknesses - even though the X-ray flux is reduced to minimize this effect. Moreover, we observe the opening of a hysteresis while the number of layers increases. The most striking is the clear opening of a thermal hysteresis of 35 ± 9 K for a 3 ML film. To the best of our knowledge, this is the first time that a so-wide bistability is achieved for such a thin SCO molecular layer. The bistability range becomes even larger as we increase the molecular coverage.

In order to qualitatively understand the influence of the substrate on the behaviour of spin-crossover molecular ultrathin films, we have performed simulations of appropriate samples within the framework of a 3D mechanoelastic approach with an Arrhenius Monte Carlo procedure, as explained in the SI. The system is modeled as a set of balls in a face-centered cubic configuration, with different radius in the HS and LS states. They are all connected by springs - six in the same plan, three above and three below. The spring stiffness constant between molecules (k_{mol}) encodes the interaction between spin-crossover units. Then, to mimic the interaction with the Cu(111) surface, a spring constant was imposed between the first molecular layer and the substrate with a stiffness constant k_s.[26] To find a realistic set of parameters k_{mol}, k_s and Monte Carlo time (MC time) which determine ΔT, T_{tr} and x_{HS}^{res}, we have done a series of tests. We first simulated the thermal behavior of the bulk (approximated here as a free system composed of eleven layers without substrate) as shown in Figure 3 in grey to fixed values of MC time and k_{mol} giving a good estimation of T_{tr} and ΔT. Note that the shape of the transition curves between experiment and simulation are different. The asymmetric and gradual transition of **(1)** is uncommon and still unexplained. It could be due to anisotropy in the molecular crystal or to domains of different

crystallinity that are not included in the simulation. We have then determined a value of k_s and the activation energy (i.e., E_a) that reproduces, at least qualitatively, the experimental measurements. Figure 3 presents the hysteresis cycles obtained for $k_{mol} = 5.2$ N.m^{-1}, $k_s = 0.5$ N.m^{-1}, $E_a = 600$ K for which the best qualitative agreement with experimental data is obtained. A temperature sweep rate of 10 MC time/K, for which kinetic effects can be still present[37] as the time scaling in Monte Carlo methods are typically remedied by experimental input.[38] Other relevant parameters are $\Delta H = 1698 \times 10^{-23}$ J and $\Delta S = 8.86 \times 10^{-23}$ J.K^{-1} (or $g = 1096$) and $\tau = 1000$ (scaling constant for the switching probability which ensures that the probability is always below 1). These values are kept constant for the rest of our simulations, if not stated otherwise. A qualitative agreement with experimental data is observed. Indeed, it reproduces well that the thicker the molecular layer, the lower x_{HS}^{res} and the higher T_{tr} and ΔT.

A careful analysis of simulation results reveal the existence of two main competitions between the parameters in the system. On one side, there is a competition between the HS-LS relaxation and the stresses induced by the layers with the tendency to maintain the system in the HS state. This is somewhat similar to the competition between relaxation and photoexcitation during light-induced thermal hysteresis (with the notable exception that the photoexcitation rate is constant, while the stresses increase with decreasing HS). With regard to this competition, it is evident that a larger k_s induces a larger residual HS fraction. On the other side, there is a competition between the size (i.e., the number of layers), which normally plays towards the increase of the hysteresis width and the average values of stresses due to the substrate felt by all the spin-crossover molecules, which decrease with the size. Due to this second competition, T_{tr} tends to increase for a larger number of layers (because the descending branch decreases faster due to less constraints, while the ascending branch goes up slower due to the larger size). The residual fraction depends mainly on the $\frac{k_s}{k_{mol}}$ ratio, but also on the temperature sweep rate and on the E_a. A larger temperature sweep rate will lead to the increase of the residual fraction, but also to a larger hysteresis width.

Finally, E_a modulates the relaxation rate and due to the above-mentioned relaxation-stress competition, may dramatically affect the equilibrium fractions. The smaller the E_a is, the smaller the residual fraction will be.

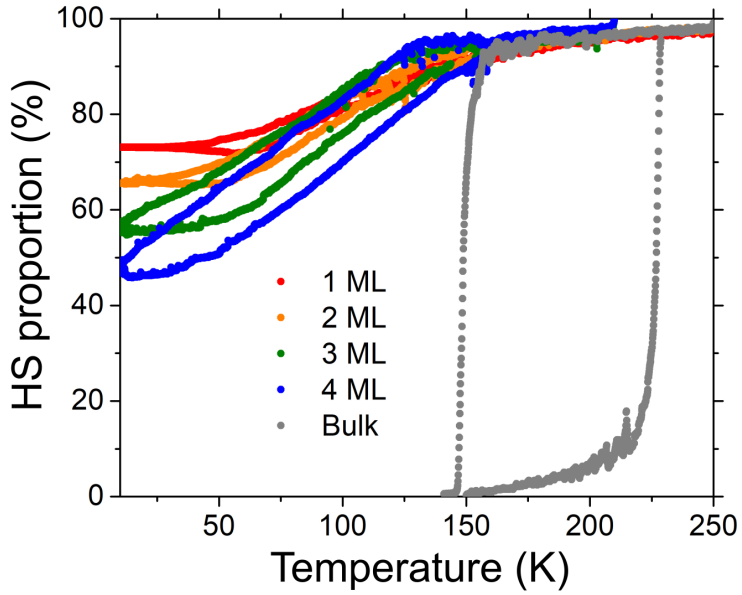

Figure 3: Calculated fraction of HS molecules as a function of temperature for k_{mol} = 5.2 N.m^{-1}, k_s = 0.5 N.m^{-1}, MC time = 0.1 K/step. Red: 1 ML; Orange: 2 ML; Green: 3 ML; Blue: 4 ML; Grey : Bulk (k_s = 0 N.m^{-1}).

To better understand the role of the substrate and the thickness on x_{HS}^{res}, we have performed simulations of the relaxed state at low temperature (cf. Figure 4). Figure 4a shows the evolution of x_{HS}^{res} as we increase the number of layers for k_s = 0.5 N.m^{-1}. As discussed for Figure 3, the increase of the number of molecular layer leads to a decrease of the final HS proportion. For this (k_{mol}, k_s) set, the complete thermal transition to the LS state is expected for a thickness superior to that of 8 ML. At this point, it is important to note that x_{HS}^{res} as measured is an average quantity over the different molecular layers. To understand how the x_{HS}^{res} is distributed from one layer to the other, the proportion of HS molecules can be decomposed in the different layers of the film, as it is represented in Figure 4b for the same k_s. Interestingly, we find that the proportion of HS molecules is higher close to the metallic surface, what is explained by the epitaxial constraint imposed by k_s. But remarkably, the interfacial HS proportion decreases when the number of topmost layers increases, what

shows that the overall HS fraction is a delicate balance between the interfacial constraint and the cooperativity imposed by the other layers. We present in the SI the results for k_s = 0.1 N.m^{-1} and k_s = 3.0 N.m^{-1} where it is clear that the lower the k_s, the more efficient the cooperativity induced by the topmost layers. This effect is summarized in Figure 4c that presents the fraction of HS molecules in the interfacial layer as a function of the film thickness and for different k_s values. As discussed previously, for all the values of k_s, the proportion of HS molecules in the interfacial layer decreases when the total number of layers increases due to the competition between the forces generated by the substrate and those coming from the topmost layers. For a very low value (k_s = 0.1 N.m^{-1}) as compared to k_{mol}, we can observe a complete transition of the interface layer for a 3 ML thickness. On the contrary, for a large value (k_s = 3.0 N.m^{-1}) which is of the same order of magnitude as k_{mol}, the residual fraction on the first layer does not decrease significantly with the thickness because the molecule-substrate interaction overcomes the molecular interlayer interaction. In this latter case, we expect a strong gradient of HS proportion with the thickness, what can have important consequences on the charge and spin transport properties of such ultrathin films.

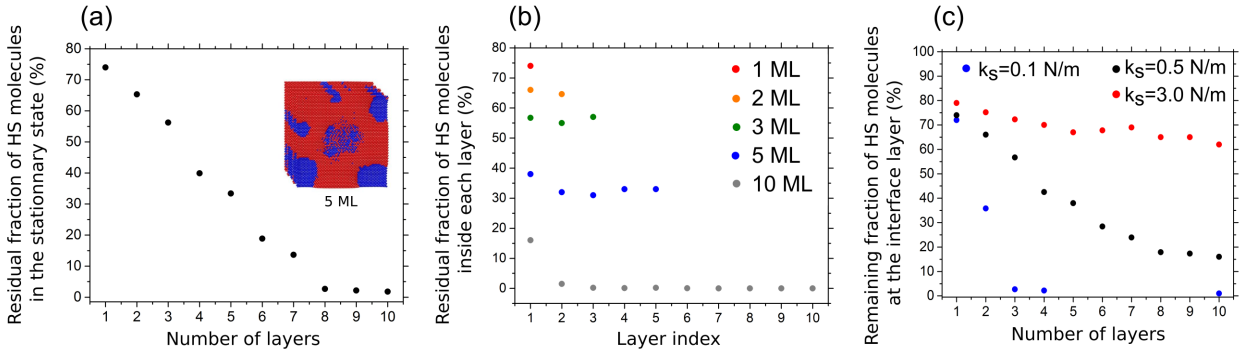

Figure 4: Monte Carlo Arrhenius simulations for: a) Residual fraction of HS molecules as a function of the number of layers for k_s = 0.5 N.m^{-1}. In inset: Snapshot of the residual fraction of HS molecules for the 5 ML system. b) Decomposition of the residual fraction of HS molecules inside each layer. Red: 1 ML; Orange: 2 ML; Green: 3 ML; Blue: 5 ML; Grey: 10 ML. c) Evolution of the remaining fraction of HS molecules in the interfacial layer as a function of the total number of layers. Blue: k_s = 0.1 N.m^{-1}; Black: k_s = 0.5 N.m^{-1}; Red: k_s = 3.0 N.m^{-1}.

As a conclusion, we have shown by means of X-ray absorption spectroscopy that spin-crossover molecular films of $Fe^{II}((3,5\text{-}(CH_3)_2Pz)_3BH)_2$ display a clear thermal bistability for thicknesses above 3 ML when grown on Cu(111). We also found that the transition temperature is rapidly increasing with the thickness whereas the fraction of residual HS molecules at low temperature is decreasing. All those results can be well reproduced by a mechanoelastic model that includes a specific interaction with the substrate. A detailed analysis of such simulations shows that for a strong enough interaction with the substrate, the HS proportion is not homogeneous over the film thickness, what can be important for electronic transport properties through such molecular layers.

Experiments :

The Cu(111) single crystal (6.5 × 5.5 mm) is cleaned by multiple cycles of sputtering (U=600 V, $P_{Ar^+} = 2.10^{-6}$ mbar) followed by an annealing at 700 K in UHV chamber (base pressure P = 3.10^{-10} mbar). STM images show a perfectly clean surface prior to deposition with terrace sizes up to 150 nm. The powder deposition of **(1)** is achieved under UHV (P = 5.10^{-9} mbar) from a homemade Knudsen cell with a 0.5 cm^3 crucible heated at around 358 K. In order to get different thicknesses on the same sample, prior to the deposition, a movable shadow mask made by a tantalum foil was placed a few mm from the sample surface, allowing to define different areas on one sample. We realized one sample with three regions of around 2 mm wide each for 0.9±0.2 ML, 1.7±0.4 ML, 3.0±0.7 ML and an other one with 2 areas of around 3 mm and 2 mm wide for 3.8±1.0 ML and 5.3±1.3 ML, respectively. Thus, the temperature ramps are the same for a given sample allowing a direct comparison of the results. As previously reported by Zhang et. al,[20] the calibration of the thicknesses is based on a quantitative correspondence between coverage in several submonolayer STM images and XAS jump-to–edge intensity at room temperature as a reference to deduce the thicknesses of the other regions. The error bar reflects the coverage fluctuations from image to image in the submonolayer range. A thorough STM analysis confirmed the integrity as

well as the self-assembly of **(1)** on Cu(111).[20,41] The prepared sample is transferred in a homemade vacuum suitcase with pressure in the low 10^{-10} mbar and transported within few hours to the X-ray absorption spectroscopy (XAS) measurement on beamline DEIMOS, Synchrotron SOLEIL. For all the samples, the XAS is performed with circularly polarized X-ray with an energy resolution better than 150 meV. The total incoming photon flux on the different samples is typically 10^8 photons.s^{-1}.mm^{-2}. The sample is placed with the X-ray incident direction perpendicular to its surface. A total electron yield mode (drain current measurement) is used to measure the Fe^{II} $L_{2,3}$ edges. The beam was 0.8 mm large, i.e. large enough to have a low fluence but small enough to probe an area with a given thickness.

Simulation :

In the present simulation, spin-crossover molecules are represented as balls with different radii in HS and LS states, situated at the sites of a face-centred cubic lattice with open boundary conditions, situated on a surface formed by neutral molecules. Each spin-crossover molecule (except those at the surface and on the first layer) is linked to its closest six neighbouring molecules on the same layer (plane), to three molecules in the plane below and to other three in the plane above by springs with an elastic constant k_{mol}, which modulates the cooperativity of the system. In addition, each spin-crossover molecule on the first layer is linked to three substrate molecules configuration by springs with an elastic constant k_s.
Each spin-crossover layer is composed of 3030 molecules; the surface is somewhat larger, to ensure that all SCO molecules, including those on the edges are linked with three surface molecules. In the initial HS state, all springs have their natural length (they are neither compressed or elongated). The intrinsic parameters of the system are : $\Delta H = 1698 \times 10^{-23}$ J and $\Delta S = 8.86 \times 10^{-23}$ J.K^{-1} (or g = 1096), thus giving a thermal transition temperature $T_c = \frac{\Delta H}{k_B \ln g}$ of around 189.5 K. Spin-crossover molecules in their HS state and surface molecules have a radius of 0.22 nm, while molecules in LS state have a radius of

0.20 nm. The distance between centers of molecule is 1 nm in LS state (1.04 nm in HS state) which results in an uncompressed length of the springs of 0.6 nm. The Arrhenius Monte-Carlo procedure we have used is described in reference.[37,39,40]

Acknowledgement

This project has received funding from the European Union's Horizon 2020 research and innovation programme undergrant agreement No [766726]. The work of C.E. was supported by a grant of the Romanian Ministry of Research, Innovation and Digitization, CNCS/CCCDI – UEFISCDI, project number PN-III-P4-ID-PCE-2020-1946, within PNCDI III. We thank Aurélie Covasso for assistance with the UHV suitcase. We acknowledge SOLEIL for provision of Synchrotron radiation facilities and we would like to thank DEIMOS staff for assistance in using the beamline, especially Florian Leduc for support with UHV chamber preparation.

Supporting Information Available

The following files are available free of charge :
Supporting Information : Thermal Bistability of an Ultrathin Film of Iron(II) Spin-Crossover Molecules Directly Adsorbed on a Metal Surface

- Evolution of the XAS signal with the temperature : Determination of HS proportion from XAS spectrum, temperature correction, movies of the evolution of the XAS signal with the temperature, the 3.8 $\pm$ 1.0 ML coverage, values of x_{HS}^{res}, T_{tr} and ΔT.
- Monte Carlo simulation of the evolution of the HS proportion with the temperature : movies of the thermal hysteresis, the relaxation curves.

References

(1) Bousseksou, A.; Molnár, G.; Matouzenko, G. Switching of Molecular Spin States in Inorganic Complexes by Temperature, Pressure, Magnetic Field and Light: Towards Molecular Devices: Switching of Molecular Spin States in Inorganic Complexes. *Eur. J. Inorg. Chem.* **2004**, *2004*, 4353–4369.

(2) Real, J. A.; Gaspar, A. B.; Muñoz, M. C. Thermal, Pressure and Light Switchable Spin-Crossover Materials. *Dalton Trans.* **2005**, 2062–2079.

(3) Bousseksou, A.; Molnár, G.; Salmon, L.; Nicolazzi, W. Molecular Spin-Crossover Phenomenon: Recent Achievements and Prospects. *Chem. Soc. Rev.* **2011**, *40*, 3313–3335.

(4) Gütlich, P.; Gaspar, A. B.; Garcia, Y. Spin State Switching in Iron Coordination Compounds. *Beilstein J. Org. Chem.* **2013**, *9*, 342–391.

(5) Halcrow, M. A. The Spin-States and Spin-Transitions of Mononuclear Iron(II) Complexes of Nitrogen-Donor Ligands. *Polyhedron* **2007**, *26*, 3523–3576.

(6) Brooker, S. Spin-Crossover with Thermal Hysteresis: Practicalities and Lessons Learnt. *Chem. Soc. Rev.* **2015**, *44*, 2880–2892.

(7) Kahn, O. Spin-Transition Polymers: From Molecular Materials Toward Memory Devices. *Science* **1998**, *279*, 44–48.

(8) Larionova, J.; Salmon, L.; Guari, Y.; Tokarev, A.; Molvinger, K.; Molnár, G.; Bousseksou, A. Towards the Ultimate Size Limit of the Memory Effect in Spin-Crossover Solids. *Angew. Chem., Int. Ed.* **2008**, *47*, 8236–8240.

(9) Holovchenko, A.; Dugay, J.; Giménez-Marqués, M.; Torres-Cavanillas, R.; Coronado, E.; van der Zant, H. S. J. Near Room-Temperature Memory Devices Based on Hybrid Spin-Crossover@SiO_2 Nanoparticles Coupled to Single-Layer Graphene Nanoelectrodes. *Adv. Mater.* **2016**, *28*, 7228–7233.

(10) Lefter, C.; Davesne, V.; Salmon, L.; Molnár, G.; Demont, P.; Rotaru, A.; Bousseksou, A. Charge Transport and Electrical Properties of Spin Crossover Materials: Towards Nanoelectronic and Spintronic Devices. *Magnetochemistry* **2016**, *2*, 18.

(11) Senthil Kumar, K.; Ruben, M. Emerging Trends in Spin-Crossover (SCO) Based Functional Materials and Devices. *Coord. Chem. Rev.* **2017**, *346*, 176–205.

(12) Galán-Mascarós, J. R.; Coronado, E.; Forment-Aliaga, A.; Monrabal-Capilla, M.; Pinilla-Cienfuegos, E.; Ceolin, M. Tuning Size and Thermal Hysteresis in Bistable Spin Crossover Nanoparticles. *Inorg. Chem.* **2010**, *49*, 5706–5714.

(13) Shepherd, H. J.; Molnár, G.; Nicolazzi, W.; Salmon, L.; Bousseksou, A. Spin Crossover at the Nanometre Scale. *Eur. J. Inorg. Chem. Chemistry* **2013**, *2013*, 653–661.

(14) Devid, E. J.; Martinho, P. N.; Kamalakar, M. V.; Šalitroš, I.; Prendergast, U.; Dayen, J.-F.; Meded, V.; Lemma, T.; González-Prieto, R.; Evers, F.; Keyes, T. E.; Ruben, M.; et al. Spin Transition in Arrays of Gold Nanoparticles and Spin Crossover Molecules. *ACS Nano* **2015**, *9*, 4496–4507.

(15) Gruber, M.; Davesne, V.; Bowen, M.; Boukari, S.; Beaurepaire, E.; Wulfhekel, W.; Miyamachi, T. Spin State of Spin-Crossover Complexes: From Single Molecules to Ultrathin Films. *Phys. Rev. B: Condens. Matter Mater. Phys.* **2014**, *89*, 195415..

(16) Gopakumar, T. G.; Bernien, M.; Naggert, H.; Matino, F.; Hermanns, C. F.; Bannwarth, A.; Mühlenberend, S.; Krüger, A.; Krüger, D.; Nickel, F.; et al. Spin-Crossover Complex on Au(111): Structural and Electronic Differences Between Mono- and Multilayers. *Chem. - A Eur. J.* **2013**, *19*, 15702–15709.

(17) Bernien, M.; Naggert, H.; Arruda, L. M.; Kipgen, L.; Nickel, F.; Miguel, J.; Hermanns, C. F.; Krüger, A.; Krüger, D.; Schierle, E.; et al. Highly Efficient Thermal and Light-Induced Spin-State Switching of an Fe(II) Complex in Direct Contact with a Solid Surface. *ACS Nano* **2015**, *9*, 8960–8966.

(18) Bairagi, K.; Bellec, A.; Fourmental, C.; Iasco, O.; Lagoute, J.; Chacon, C.; Girard, Y.; Rousset, S.; Choueikani, F.; Otero, E.; et al. Temperature-, Light-, and Soft X-ray-Induced Spin Crossover in a Single Layer of Fe^{II}-Pyrazolylborate Molecules in Direct Contact with Gold. *J. Phys. Chem. C* **2018**, *122*, 727–731.

(19) Rohlf, S.; Grunwald, J.; Jasper-Toennies, T.; Johannsen, S.; Diekmann, F.; Studniarek, M.; Berndt, R.; Tuczek, F.; Rossnagel, K.; Gruber, M. Influence of Substrate Electronic Properties on the Integrity and Functionality of an Adsorbed Fe(II) Spin-Crossover Compound. *J. Phys. Chem. C* **2019**, *123*, 17774–17780.

(20) Zhang, L.; Tong, Y.; Kelai, M.; Bellec, A.; Lagoute, J.; Chacon, C.; Girard, Y.; Rousset, S.; Boillot, M.; Rivière, E.; et al. Anomalous Light-Induced Spin-State Switching for Iron(II) Spin-Crossover Molecules in Direct Contact with Metal Surfaces. *Angew. Chem., Int. Ed.* **2020**, *59*, 13341–13346.

(21) Ridier, K.; Molnár, G.; Salmon, L.; Nicolazzi, W.; Bousseksou, A. Hysteresis, Nucleation and Growth Phenomena in Spin-Crossover Solids. *Solid State Sciences* **2017**, *74*, A1–A22.

(22) Kipgen, L.; Bernien, M.; Ossinger, S.; Nickel, F.; Britton, A. J.; Arruda, L. M.; Naggert, H.; Luo, C.; Lotze, C.; Ryll, H.; et al. Evolution of Cooperativity in the Spin Transition of an Iron(II) Complex on a Graphite Surface. *Nat. Commun.* **2018**, *9*, 2984.

(23) Rubio-Giménez, V.; Bartual-Murgui, C.; Galbiati, M.; Núñez-López, A.; Castells-Gil, J.; Quinard, B.; Seneor, P.; Otero, E.; Ohresser, P.; Cantarero, A.; et al. Effect of Nanostructuration on the Spin-Crossover Transition in Crystalline Ultrathin Films. *Chem. Sci.* **2019**, *10*, 4038–4047.

(24) Davesne, V. et al. Hysteresis and Change of Transition Temperature in Thin films

of Fe{[Me_2Pyrz]$_3$BH}$_2$, a New Sublimable Spin-Crossover Molecule. *J. Chem. Phys.* **2015**, *142*, 194702.

(25) Jiang, X.; Hao, G.; Wang, X.; Mosey, A.; Zhang, X.; Yu, L.; Yost, A. J.; Zhang, X.; DiChiara, A. D.; N'Diaye, A. T.; et al. Tunable Spin-State Bistability in a Spin Crossover Molecular Complex. *J. Phys.: Condens. Matter* **2019**, *31*, 315401.

(26) Fourmental, C.; Mondal, S.; Banerjee, R.; Bellec, A.; Garreau, Y.; Coati, A.; Chacon, C.; Girard, Y.; Lagoute, J.; Rousset, S.; et al. Importance of Epitaxial Strain at a Spin-Crossover Molecule–Metal Interface. *J. Phys. Chem. Lett* **2019**, *10*, 4103–4109.

(27) Ossinger, S.; Naggert, H.; Kipgen, L.; Jasper-Toennies, T.; Rai, A.; Rudnik, J.; Nickel, F.; Arruda, L. M.; Bernien, M.; Kuch, W.; et al. Vacuum-Evaporable Spin-Crossover Complexes in Direct Contact with a Solid Surface: Bismuth versus Gold. *J. Mater. Chem. C* **2017**, *121*, 1210–1219.

(28) Ossinger, S.; Kipgen, L.; Naggert, H.; Bernien, M.; Britton, A. J.; Nickel, F.; Arruda, L. M.; Kumberg, I.; Engesser, T. A.; Golias, E.; et al. Effect of Ligand Methylation on the Spin-Switching Properties of Surface-Supported Spin-Crossover Molecules. *J. Phys.: Condens. Matter* **2020**, *32*, 114003.

(29) Slichter, C. P.; Drickamer, H. G. Pressure-Induced Electronic Changes in Compounds of Iron. *J. Chem. Phys.* **1972**, *56*, 2142–2160.

(30) Boukheddaden, K.; Linares, J.; Spiering, H.; Varret, F. One-Dimensional Ising-Like Systems: an Analytical Investigation of The Static and Dynamic Properties, Applied to Spin-Crossover Relaxation. *Eur. Phys. J. B* **2000**, *15*, 317–326.

(31) Delgado, T.; Enachescu, C.; Tissot, A.; Guénée, L.; Hauser, A.; Besnard, C. The Influence of the Sample Dispersion on a Solid Surface in the Thermal Spin Transition of [Fe(pz)Pt(CN)$_4$] Nanoparticles. *Phys. Chem. Chem. Phys.* **2018**, *20*, 12493–12502.

(32) Bairagi K.; Iasco O.; Bellec A.; Kartsev A.; Li D.; Lagoute J.; Chacon C.; Girard Y.; Rousset S.; Miserque F.; et al. Molecular-Scale Dynamics of Light-Induced Spin Crossover in a Two-Dimensional Layer. *Nat. Commun.* **2016**, *7*, 12212.

(33) Iasco, O.; Boillot, M.-L.; Bellec, A.; Guillot, R.; Rivière, E.; Mazerat, S.; Nowak, S.; Morineau, D.; Brosseau, A.; Miserque, F.; et al. The Disentangling of Hysteretic Spin Transition, Polymorphism and Metastability in Bistable Thin Films Formed by Sublimation of bis(scorpionate) Fe(II) Molecules. *J. Mater. Chem. C* **2017**, *5*, 11067–11075.

(34) Beniwal, S.; Zhang, X.; Mu, S.; Naim, A.; Rosa, P.; Chastanet, G.; Létard, J.-F.; Liu, J.; Sterbinsky, G. E.; Arena, D. A.; et al. Surface-Induced Spin State Locking of the $[Fe(H_2B(pz)_2)_2(bipy)]$ Spin Crossover Complex. *J. Phys.: Condens. Matter* **2016**, *28*, 206002.

(35) Warner, B.; Oberg, J. C.; Gill, T. G.; El Hallak, F.; Hirjibehedin, C. F.; Serri, M.; Heutz, S.; Arrio, M.-A.; Sainctavit, P.; Mannini, M.; et al. Temperature- and Light-Induced Spin Crossover Observed by X-ray Spectroscopy on Isolated Fe(II) Complexes on Gold. *J. Phys. Chem. Lett* **2013**, *4*, 1546–1552.

(36) Collison, D.; David Garner, C.; M. McGrath, C.; Frederick W. Mosselmans, J.; D. Roper, M.; M. W. Seddon, J.; Sinn, E.; A. Young, N. Soft X-ray induced excited spin state trapping and soft X-ray photochemistry at the iron $L_{2,3}$ edge in $[Fe(phen)_2(NCS)_2]$ and $[Fe(phen)_2(NCSe)_2]$ (phen = 1,10-phenanthroline). *J. Chem. Soc., Dalton Trans.* **1997**, 4371–4376.

(37) Stoleriu, L.; Chakraborty, P.; Hauser, A.; Stancu, A.; Enachescu, C. Thermal Hysteresis in Spin-Crossover Compounds Studied within the Mechanoelastic Model and its Potential Application to Nanoparticles. *Phys. Rev. B: Condens. Matter Mater. Phys.* **2011**, *84*, 134102.

(38) Bertoni, R.; Lorenc, M.; Cailleau, H.; Tissot, A.; Laisney, J.; Boillot, M.-L.; Stoleriu, L.;

Stancu, A.; Enachescu, C.; Collet, E. Elastically Driven Cooperative Response of a Molecular Material Impacted by a Laser Pulse. *Nat. Mater* **2016**, *15*, 606–610.

(39) Enachescu, C.; Hauser, A. Study of Switching in Spin Transition Compounds within the Mechanoelastic Model with Realistic Parameters. *Phys. Chem. Chem. Phys.* **2016**, *18*, 20591–20599.

(40) Enachescu, C.; Nicolazzi, W. Elastic Models, Lattice Dynamics and Finite Size Effects in Molecular Spin-Crossover Systems. *C. R. Chim.* **2018**, *21*, 1179–1195.

(41) Kelai, M.; Cahier, B.; Atanasov, A.; Neese, F.; Tong, Y.; Zhang, L.; Bellec, A.; Iasco, O.; Rivière, E.; Guillot, R. et al. Robust Magnetic Anisotropy of a Monolayer of Hexacoordinate Fe(II) Complexes Assembled on Cu(111) *Inorg. Chem. Front.* **2021**, *8*, 2395–2404.